Local Binary Patterns to Evaluate Trabecular Bone Structure from Micro-CT Data: Application to Studies of Human Osteoarthritis

Jérôme Thevenot, Jie Chen, Mikko Finnilä, Miika Nieminen, Petri Lehenkari, Simo Saarakkala and Matti Pietikäinen

University of Oulu / Oulu University Hospital, Oulu, Finland

Abstract. Osteoarthritis (OA) causes progressive degeneration of articular cartilage and pathological changes in subchondral bone. These changes can be assessed volumetrically using micro-computed tomography (μCT) imaging. The local descriptor, i.e. local binary pattern (LBP), is a new alternative solution to perform analysis of local bone structures from μCT scans. In this study, different trabecular bone samples were prepared from patients diagnosed with OA and treated with total knee arthroplasty. The LBP descriptor was applied to correlate the distribution of local patterns with the severity of the disease. The results obtained suggest the appearance and disappearance of specific oriented patterns with OA, as an adaptation of the bone to the decrease of cartilage thickness. The experimental results suggest that the LBP descriptor can be used to assess the changes in the trabecular bone due to OA.

Keywords: Bone Structural Analysis, Micro-CT, Osteoarthritis, Multiscale LBP

1 Introduction

The local binary pattern (LBP) descriptor [25][28] has been widely used for object recognition, image segmentation, texture analysis, face analysis, *et al.* in computer vision field. However, most of the LBP studies are based on texture and material classification [25][30], and the possibilities offered by the LBP descriptor for structural analysis of objects in the medical field are still poorly known. In general, the low sensitivity of the LBP for monotonic greyscale variations [24] makes it ideal for medical image processing. Furthermore, the LBP descriptor offers the possibility to assess the distribution of local patterns within a region/volume of interest both in 2D and 3D. Despite these facts very few LBP studies have been performed for 3D data obtained by conventional medical 3D imaging techniques, such as computed tomography (CT) or magnetic resonance imaging (MRI).

The nature of bone tissue, and especially its inner architecture, makes it a perfect candidate for structural analysis. As the bone adapts itself to environmental factors, the changes in its structure not only give information on its

strength, but also provide symptomatic indications of diseases [35]. As such, CT images has been used to assess the structural bone alterations in osteoporosis [33] or in osteoarthritis (OA) [6]. OA is a disease of the whole joint primarily causing degeneration of the articular cartilage and remodeling of subchondral bone. With current clinical diagnostic techniques, the disease is often diagnosed at the end stage when the joint replacement surgery is the only effective treatment available. In OA the subchondral bone is specifically affected by sclerosis and undergoes structural changes such as the formation of osteophytes and bone cysts [4]. It has been even suggested that the structural bone changes in OA might occur before the changes at the articular cartilage [5]. However, despite some evidence that the changes in subchondral bone could contribute to the development of OA [12][13][23][19], clinical diagnostic methods mostly focus on the cartilage alone by measuring its erosion and degeneration. Following this clinical trend, a recent histopathological method to grade the severity of OA at the tissue level, *i.e.* OARSI grading system, is assessing the depth and extent of the lesions in the articular cartilage [29]. The high reliability and repeatability of the OARSI grading system [9][27] suggest this method to be a consistent reference for comparative studies assessing OA at different stages of the disease.

Micro-computed tomography (μCT) is an imaging technique similar to clinical CT, but at micro-scale level instead of macro-scale level. A significant advantage of the LBP method if applied to μCT scans is its ability to take into account the impact of partial volume effect. The partial volume effect is always a downside of the conventional analysis of bone structure, as a result of the binarization of the data for volumetric reconstruction. Eventually, μCT allows to analyze the inner structure of bone (see Fig. 1 up) with high resolution, enabling to study the size, organization and connectivity of individual bone fibers. The analysis of μCT data allows to assess the micro-level changes in bone structure related to the adaptation of the wear of overlying articular cartilage. In several animal studies characteristic bone microstructural changes related to OA have been reported [21][34][10][16][17]. Similar trends in human studies have been observed in microscopic studies [20][2]. However, μCT-derived bone structural parameters have yet to be compared with the severity of OA in humans.

There is an evident lack of studies involving LBP method to bone analysis, and in each case it has been based on plain radiographic imaging [15][36][14], showing already the potential of this tool to assess OA [14]. The most interesting aspect of applying the LBP method on bone microarchitecture is to obtain local distribution of patterns on high amount of data for each sample.

The aim of this study was to establish a new protocol to assess the local changes in bone structure using LBP descriptor and to correlate them with the severity of OA assessed by OARSI grading as a ground truth. The procedure has been divided in two parts: the selection of relevant pixels by using multiscale LBP to assess the continuity of the patterns, and the grouping of the patterns based on both their orientation and their amount of markers. The methodological concepts and results introduced here have been performed in 2D slice-by-slice as a preliminary study before the development of real volumetric analysis.

2 LBP Method to Perform Bone Structural Analysis from Micro CT data

2.1 Background

In this section, we will present the background of the bone structural analysis from μCT data. After that, we describe the existing methods and their limitations. The bone includes two compartments: the trabecular bone and the cortical bone surrounding it (see Fig. 5). While the cortical compartment is more compact and mainly corresponds the bending resistance of the bone [31], the trabecular compartment is metabolically more active and affected by remodeling [35]. From the structural point of view, the adaptation of the internal compartment to environmental loading conditions makes the trabecular bone a crucial region of interest for analysis of structural changes.

Micro-computed tomography is an imaging method enabling to obtain volumetric data of microstructures [3]. Briefly, X-ray transmission measurements are used to create cross-sections of a physical object, similarly to clinical CT but at higher resolutions (<100 microns). While applied to bone analysis, it allows to visualize the trabecular structures and obtain information on the density of the bone. The average grey level value within a region of interest is also correlated to bone strength. The grey level value of each pixels for each scan is highly dependent on the mineralization of the structures: poorly mineralized structure (*i.e.* fibers being resorbed or created) will have a lower grey level value than highly mineralized structures. Another phenomenon affecting the grey level value of a pixel is the partial volume effect [32]: this phenomenon occurs for features not being totally within the slice thickness of the considered image or smaller than the pixel size, resulting in a lowered grey level value of the pixels affected. This peculiar event is expected to be more likely at the edges of the fibers, areas the most affected by remodeling. Another artefact in CT analysis is the beam hardening [22], causing the edges of an object to appear brighter than the center: this artefact is caused by the attenuation of the X-rays. All of these artefacts deteriorate the quality of CT analysis.

Traditionally, in bone structural analysis several parameters of the trabecular bone is evaluated to indicate the bone inner architecture and its quality [3]. The conventional method consists of a binarization of the image stack by a pre-defined threshold value believed to represent the minimum gray scale value of the bone. Subsequently, volumetric representation of the structure can be reconstructed and parameters calculated from the 3D model. The most relevant parameters are the bone volume fraction representing the amount of bone reconstructed over the volume, the trabecular thickness and spacing giving indication on morphometry of trabecular bone structure, and the structure model index (SMI) categorizing the trabecular structure as plate- or rod-like.

A main limitation of the conventional method to analyze bone structure is the loss of the original pixel values. Only the information related to the location of the bone and its organization remains. Furthermore, the selection of a binarization threshold is often performed subjectively, increasing inter-repeatability

inaccuracies. Finally, image pixels/voxels representing poorly mineralized structure, or pixels affected by partial volume effect, are typically excluded from the analysis to avoid overestimation of the bone structures (as shown in Fig. 1).

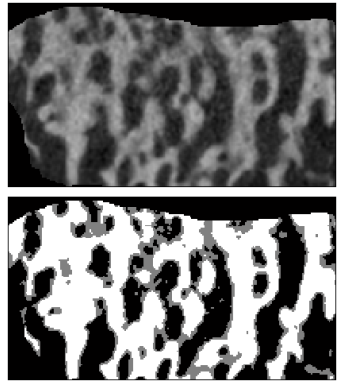

Fig. 1. up: μCT scan of a trabecular bone; **down:** white region are the bone and grey region are the pixels affected by partial volume effect / poorly mineralized. These gray regions are typically excluded from a conventional analysis of bone structure

Further parameters such as the degree of anisotropy, the fractal dimension, the trabecular number, etc. can be assessed from the analysis, but all of them are also derived from the binarized scans.

2.2 Basics of LBP

The basics of LBP [25][28] is shown in Fig. 2. The neighborhood of a center pixel is checked for evaluating the occurrences of equal/higher grey level values than in the center pixel. A specific local pattern is then determined based on the locations of these occurrences. This pattern depicts the local structure surrounding the studied pixel such as edges, contours and flat regions.

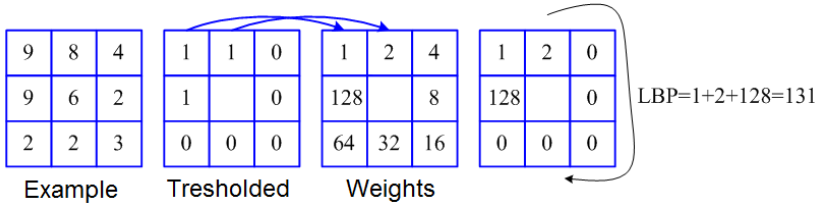

Fig. 2. Basic LBP. In the example, the center pixel (value 6) is used as a threshold. The tresholded values are then multiplied by their corresponding pixels in the weights matrix and summed to obtain the LBP value of the center pixel

The local structure of each pixels within a region of interest can be mathematically assessed by the following function:

$$LBP = \sum_{k=0}^{n-1} s(g_k - g_c)2^k, \quad s(x) = \begin{cases} 1, & x \geq 0 \\ 0, & x < 0, \end{cases} \tag{1}$$

where n is the amount of neighbors evaluated, g_k the grey level value of the k-th neighbor, and g_c the pixel value of the central (studied) pixel. Depending on the radius and amount of neighbors considered the grey level value g_k might require to be estimated by interpolation.

Eventually, the number of different patterns that can be assessed by the LBP method is related to the amount n of neighbors evaluated for each center pixel; the number of possible patterns being 2^n. While in texture analysis the full histograms of patterns might be required in the methods, in structural analysis some grouping of patterns are required to avoid redundant information of similar patterns corresponding to identical local structures assessed at different locations.

2.3 Selection of relevant pixels using multiscale LBP

Another difference between texture analysis and bone structural analysis using the LBP is the selection of the evaluated pixels. In texture analysis, every pixels within a region of interest are usually considered in the calculations. For bone structural analysis, some pre-selection has to be performed to evaluate only relevant information. As mentioned previously, in traditional analysis of bone structure from μCT scans, the images are binarized by a threshold representing the minimum grey level value of the bone. This step allows the users to separate the relevant information (the bone) from the irrelevant empty spaces. Based on this principle, structural analysis using LBP method should be applied solely to pixels located nearby or within bone structures.

The selection of relevant pixels to compute LBP features has been divided in two steps, as shown in Algorithm 1. The first step is to filter out the empty space while the second step is to filter out the isolated noise by a connection test. In our case, the Otsu method [26] was chosen to extract the foreground information representing the bone from the background representing the empty spots. However, to verify that relevant pixels with lower grey level value are not considered as background, the averaged minimum value returned by Otsu method for all the slices is lowered by an arbitrary percentage δ of its value (δ = 95% in our case), as shown in Step 1 of Algorithm 1. Here S_0 is the region filtered out the empty space by Otsu method.

An important factor in the bone structural analysis using the LBP method is to assess not only the pixels within the bone, as in traditional analysis, but also pixels that are in the neighborhood of the bone structures. This factor is crucial since the modelling and remodeling of the bone can be assessed in the surrounding of the structures (Step 2 of Algorithm 1 and Fig. 3).

Algorithm 1. The selection of relevant pixels

Input Images I obtained by μCT scan
Output The selected of relevant pixels S

Step 1 Filter out the empty space by Otsu method
1.1 $S_0 = \Phi$
1.2 Compute threshold by Otsu method g_{otsu}
1.3 For $g_c \in I$
If $g_c > \delta g_{otsu}$
S_0=S_0+$\{g_c\}$
End
End

Step 2 Filter out the isolate noise by connection test $g_{k,1}$
2.1 $S_1 = S_2 = \Phi$
Let $g_{k,1}$ be any of *k-th* neighbor at radius 1 from center pixel $\{g_c\}$; $g_{m,2}$ be *m-th* neighbor at radius 2 from g_c. *k*=0,1,...7 and *m*=0,1,...15
2.2 For $g_c \in S_0$
If $\exists\ g_{k,1} > \delta g_{otsu}$ and *k*=0,1,...7
S_1=S_1+$\{g_c\}$
End
End
2.3 Let *R* be the max distance used for connectivity test
For $g_c \in I - S_0$
If $\exists\ g_{k,1} > \delta g_{otsu}$ and $\exists\ g_{m,2} \geq \delta g_{otsu}$,
and $\parallel g_{k,1} - g_{m,2} \parallel \leq R$, *m*=0,1,...15
$S_2 = S_2$+$\{g_c\}$
End
End
2.4 $S = S_1 + S_2$

Specifically, the structures of the bone are continuous. Based on this principle, we propose using multiscale LBP method to select only bone structures and get rid of irrelevant artefacts. The selection of relevant pixels can be performed by two steps: the first one assessing the pixels within the structures, and the second assessing the pixels next to the edges of the structures. Both of the steps can be performed at multiple scales depending on the resolution of the images. In our case, we use two scales, *i.e.* it is considered that only areas with at least two consecutive pixels higher than a specific threshold are actual bone.

As shown in Step 2.4 of Algorithm 1, S is the resulting pixels, which are used for the following structure analysis using LBP. Increasing the amount of neighbors for a higher radius improves the accuracy of the method as more similar patterns can be considered. An option is to increase the amount of neighbors by 8 for each increase of radius, as suggested earlier [24].

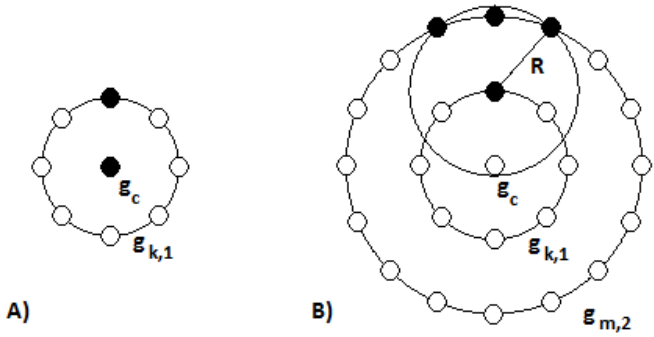

Fig. 3. Examples of center pixels considered in the analysis. Black markers have equal/higher grey level value than the threshold. **A**) Both the center pixel and one of its neighbor k have higher grey level value than the threshold. **B)** The empty center pixel is neighbor with an edge at radius 1. The continuation of the bone is validated at radius 2 within the length R (three neighbors m checked in this case)

2.4 Grouping of patterns using principal component analysis

After applying the LBP method to an image, a histogram is generated with a size corresponding to the amount of different patterns assessed. However, in bone structural analysis a large amount of assessed patterns are redundant, as they represent the same information obtained from different locations. This suggests that grouping of the patterns is required to obtain reduced histograms with truly relevant information. Therefore, we propose to group the patterns both by their main orientation, but also by taking into account the amount of markers they consist. The term marker describes a neighbor with an equal/higher grey level value than both the central pixel g_c and the threshold. The justification for this grouping can be explained as follows:
- The main orientation of the patterns provides information on the orientation of the structures of recognized bone fiber. For example, healthy bone fibers are expected to have structures organized mainly along the daily loading orientation. Structures with different orientations could suggest an adaptation of the inner architecture of the bone fiber due to extra factors.
- The amount of markers in each pattern gives information on the nature of the local structures of bone fiber. For example, if 8 neighbors are considered in the analysis a pattern with 2-3 consecutive markers will suggest a straight structure, while a pattern with more consecutive markers will suggest a corner or a spot.

Principal component analysis (PCA) is performed for each possible pattern to obtain its main orientation. A score of the PCA is assessed to exclude the patterns without a consistent orientation. For a specific pattern, the principal components of each markers were assessed and averaged by axis. Then, the score corresponded to the value of the axis with highest weight, this axis being the most affected by the location of the markers. A high value suggests a distribution sparse along this axis and eventually along the main orientation of the pattern.

To resume, this score evaluates how well the markers of a pattern are fitted towards the line representing the principal component, if the score is higher than a given threshold value, then the orientation of the pattern is not clear.

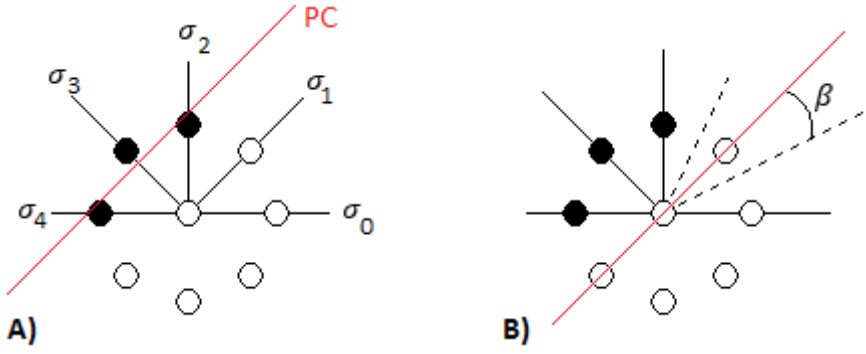

Fig. 4. Affectation of a pattern in a group. In this example, 5 different angles (σ_0 to σ_4) are used to group the patterns, as well as 8 neighbors. **A)** The principal component (PC) orientation of the pattern is defined from the 3 markers. **B)** The line representing the PC is translated to the center pixel and the angle σ_p is established within the tolerance β. For this specific case, the pattern belongs to the group (σ_1,M=3)

An example of the grouping using PCA can be seen in the Fig. 4. A group (σ_p,M) correspond to the sum of patterns with an orientation σ_p and with M markers. It is defined as follows:

$$group(\sigma_p, M) = \sum_{j=1}^{2^n} pattern_j, \quad if \begin{cases} |angle(pattern_j)| \leq \beta \\ score(pattern_j) < score_{tresh} \\ markers(pattern_j) = M, \end{cases} \tag{2}$$

with $angle(pattern_j)$ being the orientation angle of the j pattern, β the angle deviation tolerated and $score_{tresh}$ the maximum threshold value of the score from the PCA defining a clear orientation. Eventually, the amount of different groups will be defined by the amount of markers (M) and also by the number of angles (σ_p) (note that an angle σ_p being equivalent to an angle $\pi + \sigma_p$). The angle β represents the tolerance for the patterns orientation towards the angle σ_p. The angles σ_p and β are defined as such:

$$\sigma_p = \frac{\pi p}{N}, \quad with\ 0 \leq p \leq N, \tag{3}$$

$$and \quad \beta = \frac{\pi}{2N}, \tag{4}$$

with p the considered angle division and N being the amount of different angles used for grouping the patterns.

3 Experiment: Assessment of Osteoarthritis

3.1 Sample preparation, imaging and histopathology

In our experiments, 24 osteochondral samples [11] were earlier prepared from 14 patients with OA (age 76 ± 9 years: 2 males and 12 females), treated with total knee arthroplasty at Oulu University Hospital. Sample collection and their use were approved by the Ethical Committee of the Northern Ostrobothnia Hospital District, Oulu, Finland (*Diary 187/2013, Ethical Committee statement 78/2013*). Samples were prepared from tibial plateus which are always extracted during routine total knee endoprosthesis surgery. Tibial plateus were first visually classified into three categories in terms of degeneration of the articular cartilage: 1) most inviolable (or intact) cartilage, 2) moderate cartilage degeneration and wear, and 3) partly or fully exposed subchondral bone. Samples were stored in phosphate-buffered saline (PBS) for μCT imaging. While albeit samples had various cartilage thickness, they were selected from comparable anatomical area.

Osteochondral samples were scanned with μCT device at isotropic voxel size of 27.8 μm (Skyscan 1172, Bruker microCT, Kontich, Belgium). The scanned trabecular bone was located below the subchondral plate of the proximal tibia. While the bones were oriented along the proximal-distal axis during the scanning, no information regarding the medio-lateral or antero-posterior axes were available. This limitation is shown in Fig. 5.

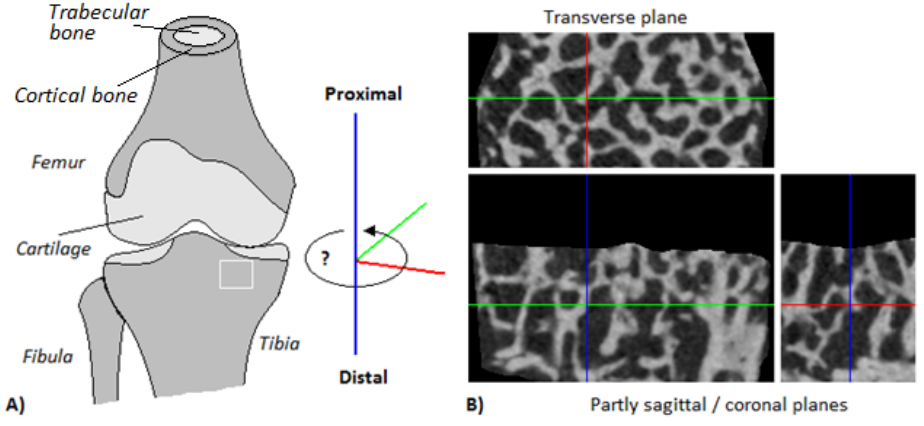

Fig. 5. A) Location of one trabecular sample (indicated by white square); only the proximal-distal axis is known. **B)** MicroCT scans of one trabecular sample along the three perpendicular planes. The lack of anatomical references suggests that the data on the lower pictures are neither fully in the sagittal nor coronal planes

After the μCT imaging, samples were formalin-fixed and decalcified in EDTA. Paraffin-embedded blocks were sectioned to 5 μm and stained with Safranin O.

Histological sections were graded from three slices by three independent evaluators according to the standardized OARSI grading system [29]. The average from three evaluators was used as a final OARSI grade in further analysis.

3.2 Data selection and structural assessment

Since only the proximal-distal axis was known, all analysis presented here were performed in both partly sagittal / coronal planes and the results obtained were averaged. Since the specific remodeling of the trabecular bone is unknown for patients at different stages of OA, it can be hypothesized that the internal architecture is affected differently along the antero-posterior axis and the medio-lateral one. Thus, considering both the perpendicular planes along the proximal-distal axis can reduce the error implied by the unknown rotation of the sample before the scanning.

The selection of the pixels implemented within the structural analysis using LBP was performed as suggested in Fig. 6. First, OTSU method within the trabecular bone was applied for each slice of both planes. Then, multiscale LBP was applied at 2 levels for the selection of relevant pixels:
- Radius 0 (the center pixel itself) and radius 1 for a center pixel with higher/equal value than g_{Otsu}.
- Radius 1 and radius 2 for a center pixel within an empty space. Similarly than in Fig. 3, 16 neighbors at radius 2 were considered. The center pixel was included in the analysis if at least one marker at radius 1 and one marker within the 3 closest neighbors at radius 2 existed.

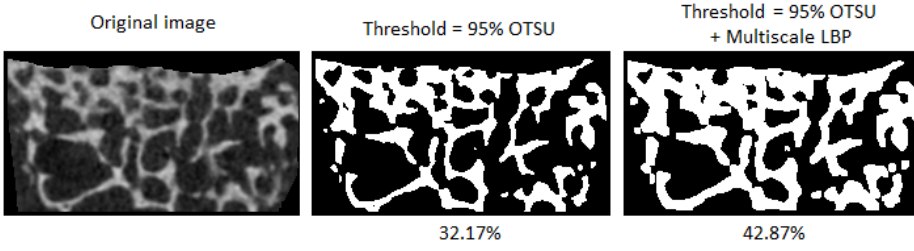

Fig. 6. Comparison between different methods to select the relevant pixels within an original μCT scan. The percentage represents the amount of selected pixels within the segmented area of the original image. Using Otsu thresholding alone gives an initial estimation for the bone pixels. Combination of Otsu thresholding and multiscale LBP selects both bone areas and the relevant surrounding pixels, and it is considered to better select relevant pixels in the analysis

Once the relevant pixels were selected, LBP analysis at radius 1 and with 8 neighbors was performed for the stack of scans. Grouping of the patterns using PCA was performed in order to evaluate 3 angles: 0, 45 and 90 ($\pm$ β=22.5). A $score_{tresh}$ of 0.75 was used in the analysis to select the oriented patterns.

This value was experimentally chosen to allow one blank neighbor (non-marker) within a set of consecutive markers of a pattern. The range of the possible angles was limited to 0-90 since the analysis was performed in 2 planes perpendicular to each other. Grouping the angles 0/180 and 45/135 by symmetry was then required to keep relevance of the results. A representation of grouping is presented in Fig. 7.

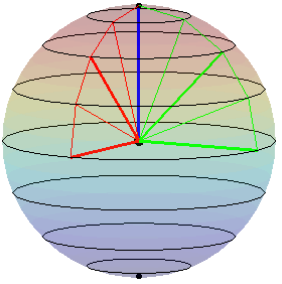

Fig. 7. Grouping of angles using PCA. Thick lines represents main angles and thin lines the deviation β

3.3 Correlations between patterns distribution and the severity of the disease

The OARSI grades of the samples were distributed from 0.89 to 6.25 (mean 3.51 ± 1.69). The intra-observer and inter-observer repeatability (CV_{rms}) of the OARSI grading were 8.78% and 11.84%, respectively. The intra-observer and inter-observer reliability (ICC) in the OARSI grading were 0.96% and 0.95%, respectively. According to previous literature [9][27], both ICC values represent an excellent reproducibility. Following this validation, the mean OARSI grade for each sample is considered as the ground truth for the stage of OA in the resulting LBP analysis.

For each sample, once the LBP method is applied to the stack of scans, the full histograms are converted to obtain the occurrences of each specific pattern as a percentage of all the patterns recognized within a volume of interest. Different parameters are assessed from the full histograms and then correlated with the OARSI grades:

- *The percentage of studied pixels*: ratio of relevant pixels used in the analysis by the total number of pixels available in the segmented trabecular bone.
- *The mean amount of markers*: corresponds to the mean value of markers for all the local patterns of the sample pooled together.
- *The amount of different patterns*: for 8 neighbors, the maximum amount of different patterns is 256. This parameter provides a count of all the local patterns recognized for a sample.

-*The entropy of local patterns*: describes the randomness of local patterns in the volume of interest. The entropy of local patterns was calculated as follows:

$$E = -\sum_{i} P_i log_2(P_i) \tag{5}$$

where P_i contains the count of a specific local pattern i occurring in the stack of scans. If an image contains only one local pattern, the entropy of the patterns within the image is zero.

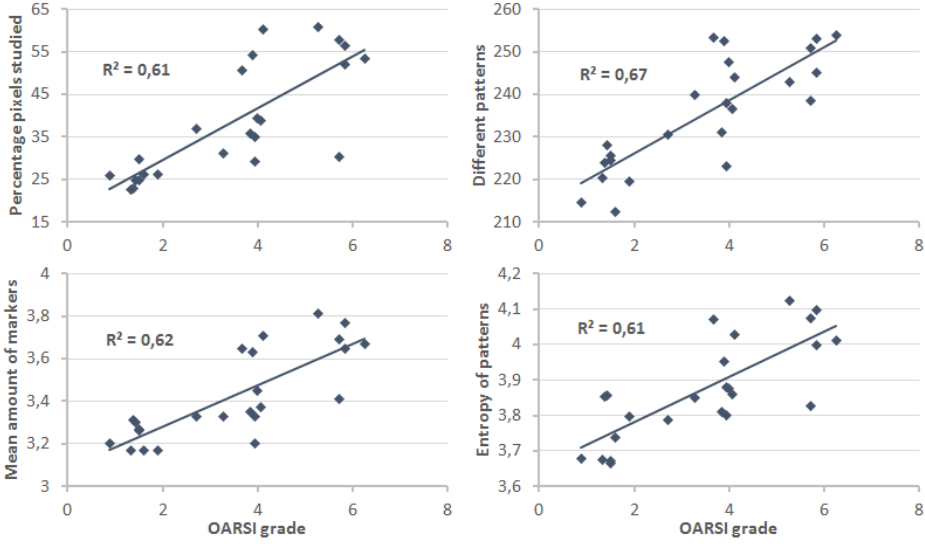

Fig. 8. Linear regression analysis between OARSI grades and trabecular bone parameters (N=24) derived from LBP analysis

Based on Fig. 8, the percentage of pixels studied is positively correlated to the severity of the disease, as suggested previously in literature [18][1]. Similarly to the results obtained in the radiographical study of Hirvasniemi *et al.* [14], the entropy of local patterns was proportional to the increase of OA level. An increase of the entropy of local patterns with OA corresponds to a higher variation in different patterns, supported by the increase of amount of different patterns, which could be explained by the appearance of bone sclerosis at higher OARSI grades [4][29].

The mean distribution of local patterns after the reduction of the histograms by grouping the patterns using PCA is shown in Fig. 9. Based on the results obtained from the Pearson correlation analysis between each group and the OARSI grades, it can be seen that the occurrence of patterns with lower amount of markers ($\leq$4) tends to disappear, while the occurrence of patterns with more markers (>4) increases. This result is also supported in Fig. 8 by the relation between the

mean amount of markers and the OARSI grade. As an explanation, while the severity of OA increases, the trabecular bone tends to create more connections to improve its strength.

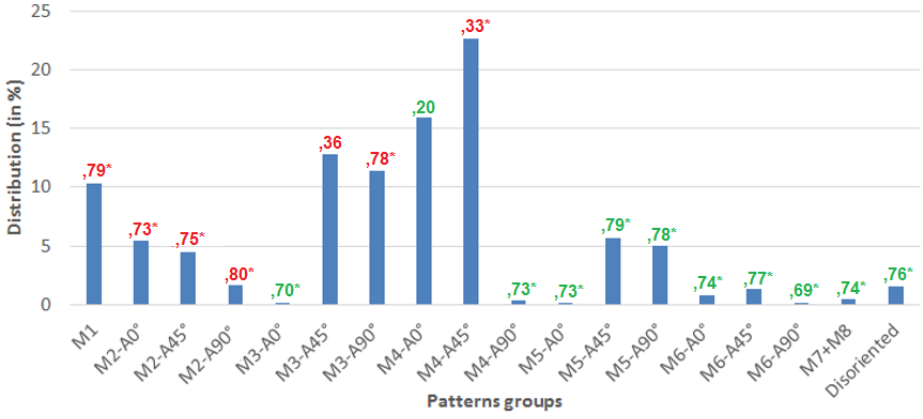

Fig. 9. Mean distribution of the pattern groups for all samples (n=24) pooled together. A group is defined by the amount of markers M and the main orientation A of its patterns. The group *Disoriented* corresponds to all the patterns without clear orientation, with markers M between 2 and 6. Correlation coefficients between OARSI grades and groups are red for a negative correlation and green for a positive one. $*p<0.001$

One interesting observation concerning the orientation of the patterns can be seen for groups with 3 markers. These groups are highly relevant since they are mainly representing straight edges of the fibers (as shown in Fig. 10).

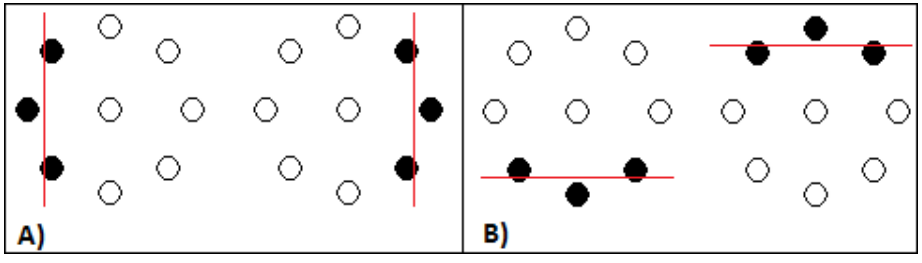

Fig. 10. Examples of patterns from two different groups with 3 markers. **A)** *M3-A90*. **B)** *M3-A0*

As expected, because the bone fibers are mostly oriented along the daily loading, the group *M3-A0* is smaller than the group *M3-A90*. However, for an increase in the severity of the disease, the group *M3-A90* decreases while the

group *M3-A0* increases, suggesting the apparition of horizontal patterns connecting trabecular fibers between each other like arches. This hypothesis is furthermore supported by the increases of groups with more markers, suggesting the creation of corners. The non-significant decrease of the group *M3-45* can be explained as it represents the transition between horizontal and vertical patterns.

The hypothesized creation of bridges (Fig. 11) between the fibers suggests a reduction of the degree of anisotropy of the trabecular bone proportionally with the disease, as previously suggested [7]. This result is furthermore supported by the decrease of trabecular separation and structure model index, suggesting the trend of the trabecular structures to change from a rode-like type towards a plate-like shape [37][8].

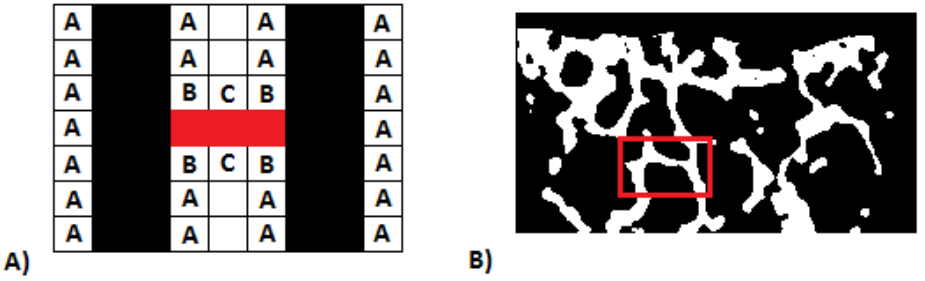

Fig. 11. A) Representation of the creation of a bridge in red between fibers in black. *A:M3-A90*, *B:M5-A45* and *C:M3-A0*. **B)** Example from a μCT slice with a bridge shown in the red rectangle

4 Conclusion

This study proposes a novel application of the local binary pattern method to perform bone structural analysis from μCT data. The experiment performed here suggests that this method can be used to assess the changes in the trabecular bone due to OA. While traditional bone structural analysis is affected by phenomena, such as partial volume effect or beam hardening, the LBP method is less subject to these issues due to its nature being based on the comparison of neighborhood intensity related to studied pixels, instead on the direct analysis of grey level values. The results obtained here are complementary to the traditional structural parameters and suggest that the assessment of other visual features could enhance the understanding of bone remodelling in OA. Further development of the present method should be performed, such as applying 3D LBP with real volumetric neighborhood analysis, using local ternary patterns method to improve the robustness, or using classifiers to estimate the severity of the disease.

Acknowledgements

This study was supported by the strategic funding of the University of Oulu, Infotech Oulu and the Academy of Finland.

References

1. Bennell, K., Creaby, M., Wrigley, T., Hunter, D.: Tibial subchondral trabecular volumetric bone density in medial knee joint osteoarthritis using peripheral quantitative computed tomography technology. Arthritis Rheum 58(9), 2776–2785 (2008)
2. Bobinac, D., Spanjol, J., Zoricic, S., Maric, I.: Changes in articular cartilage and subchondral bone histomorphometry in osteoarthritic knee joints in humans. Bone 32(3), 284–290 (2003)
3. Bouxsein, M., Boyd, S., Christiansen, B., Guldberg, R., Jepsen, K., M´u ller, R.: Guidelines for assessment of bone microstructure in rodents using micro-computed tomography. J Bone Miner Res 25(7), 1468–1486 (2010)
4. Buckwalter, J., Mankin, H.: Articular cartilage: degeneration and osteoarthritis and repair and regeneration and and transplantation. Instr.Course Lect 47, 487–504 (2012)
5. Burr, D., Gallant, M.: Bone remodelling in osteoarthritis. Nat Rev Rheumatol 8(11), 665–673 (2002)
6. Chappard, C., Peyrin, F., Bonnassie, A., Lemineur, G., Brunet-Imbault, B., Lespessailles, E., Benhamou, C.: Subchondral bone micro-architectural alterations in osteoarthritis: a synchrotron micro-computed tomography study. Osteoarthritis Cartilage 14(3), 215–223 (2006)
7. Chappard, C., Peyrin, F., Bonnassie, A., Lemineur, G., Brunet-Imbault, B., Lespessailles, E., Benhamou, C.: Subchondral bone micro-architectural alterations in osteoarthritis: a synchrotron micro-computed tomography study. Osteoarthritis Cartilage 14(3), 215–223 (2006)
8. Chiba, K., Ito, M., Osaki, M., Uetani, M., Shindo, H.: In vivo structural analysis of subchondral trabecular bone in osteoarthritis of the hip using multi-detector row ct. Osteoarthritis Cartilage 19(2), 180–185 (2011)
9. Custers, R., Creemers, L., Verbout, A., VanRijen, M., Dhert, W., Saris, D.: Reliability and reproducibility and variability of the traditional histologic histochemical grading system vs the new oarsi osteoarthritis cartilage histopathology assessment system. Osteoarthritis Cartilage 15(11), 1241–1248 (2007)
10. Ding, M., Danielsen, C., Hvid, I.: Effects of hyaluronan on three-dimensional microarchitecture of subchondral bone tissues in guinea pig primary osteoarthrosis. Bone 36(3), 489–501 (2005)
11. Finnilä, M., Aho, O.M., Tiitu, V., Thevenot, J., Rautiainen, J., Nieminen, M., Valkealahti, M., Lehenkari, P., Saarakkala, S.: Correlation of subchondral bone morphometry and oarsi grade in osteoarthritic human knee samples. Osteoarthritis Cartilage 22
12. Goldring, M., Goldring, S.: Articular cartilage and subchondral bone in the pathogenesis of osteoarthritis. Ann.N.Y.Acad.Sci 1192, 230–237 (2010)
13. Goldring, S., Goldring, M.: Bone and cartilage in osteoarthritis: is what's best for one good or bad for the other? Arthritis Res Ther 12(5), 143 (2010)
14. Hirvasniemi, J., Thevenot, J., Immonen, V., Liikavainio, T., Pulkkinen, P., Jämsä, T., Arokoski, J., Saarakkala, S.: Quantification of differences in bone texture from

plain radiographs in knees with and without osteoarthritis. Osteoarthritis Cartilage (DOI:10.1016/j.joca.2014.06.021) (2014)
15. Houam, L., Hafiane, A., Boukrouche, A., Lespessailles, E., Jennane, R.: One dimensional local binary pattern for bone texture characterization. Pattern Anal.Appl 17(1), 1–15 (2012)
16. Intema, F., Hazewinkel, H., Gouwens, D., Bijlsma, J., Weinans, H., Lafeber, F., Mastbergen, S.: In early oa and thinning of the subchondral plate is directly related to cartilage damage: results from a canine aclt-meniscectomy model. Osteoarthritis Cartilage 18(5), 691–698 (2010)
17. Intema, F., Sniekers, Y., Weinans, H., Vianen, M., Yocum, S., Zuurmond, A., DeGroot, J., Lafeber, F., Mastbergen, S.: Similarities and discrepancies in subchondral bone structure in two differently induced canine models of osteoarthritis. J Bone Miner Res 25(7), 1650–1657 (2010)
18. Kamibayashi, L., Wyss, U., Cooke, T., Zee, B.: Trabecular microstructure in the medial condyle of the proximal tibia of patients with knee osteoarthritis. Bone 17(1), 27–35 (1995)
19. Li, G., Yin, J., Gao, J., Cheng, T., Pavlos, N., Zhang, C., Zheng, M.: Subchondral bone in osteoarthritis: insight into risk factors and microstructural changes. Arthritis Res Ther 15(6), 223 (2013)
20. Matsui, H., Shimizu, M., Tsuji, H.: Cartilage and subchondral bone interaction in osteoarthrosis of human knee joint: a histological and histomorphometric study. Microsc Res Tech 37(4), 333–342 (1997)
21. Mohan, G., Perilli, E., Kuliwaba, J., Humphries, J., Parkinson, I., Fazzalari, N.: Application of in vivo micro-computed tomography in the temporal characterisation of subchondral bone architecture in a rat model of low-dose monosodium iodoacetate-induced osteoarthritis. Arthritis Res Ther 13(6), 210 (2011)
22. Nakashima, Y., Nakano, T.: Optimizing contrast agents with respect to reducing beam hardening in nonmedical x-ray computed tomography experiments. J Xray Sci Technol 22(1), 91–103 (2014)
23. neda, S.C., Roman-Blas, J., Largo, R., Herrero-Beaumont, G.: Subchondral bone as a key target for osteoarthritis treatment. Biochem Pharmacol 83(2), 315–323 (2012)
24. Ojala, T., Pietikäinen, M., Harwood, D.: A comparative study of texture measures with classification based on feature distributions. British Machine Vision Conference 25, 51–59 (1996)
25. Ojala, T., Pietikäinen, M., Mäenpää, T.: Multiresolution gray-scale and rotation invariant texture classification with local binary patterns. IEEE Transactions on Pattern Analysis and Machine Intelligence 24(7), 971–987 (2002)
26. Otsu, N.: A treshold selection method from gray-level histograms. IEEE Transactions of systems and man and cybernetics 9(1) (1979)
27. Pearson, R., Kurien, T., Shu, K., Scammell, B.: Histopathology grading systems for characterisation of human knee osteoarthritis : reproducibility and variability and reliability and correlation and validity. Osteoarthritis Cartilage 19(3), 324–331 (2011)
28. Pietikäinen, M., Hadid, A., Zhao, G., Ahonen, T.: Computer vision using local binary patterns. Springer (2011)
29. Pritzker, K., Gay, S., Jimenez, S., Ostergaard, K., Pelletier, J., Revell, P., Salter, D., Berg, W.V.: Osteoarthritis cartilage histopathology: grading and staging. Osteoarthritis Cartilage 14(1), 13–29 (2006)
30. Qi, X., YuQiao, Y., Li, C., J.Guo: Multi-scale joint encoding of local binary patterns for texture and material classification. British Machine Vision Conference (2013)

31. Seeman, E., Delmas, P.: Bone quality–the material and structural basis of bone strength and fragility. N Engl J Med 354(21), 2250–2261 (2010)
32. Souza, A., Udupa, J., Saha, P.: Volume rendering in the presence of partial volume effects. IEEE Trans Med Imaging 24(2), 223–235 (2005)
33. Thevenot, J., Hirvasniemi, J., Finnilä, M., Pulkkinen, P., Kuhn, V., Link, T., Eckstein, F., Jämsä, T., Saarakkala, S.: Trabecular homogeneity index derived from plain radiograph to evaluate bone quality. J Bone Miner Res 28(12), 2584–2591 (2013)
34. Wang, T., Wen, C., Yan, C., Lu, W., Chiu, K.: Spatial and temporal changes of subchondral bone proceed to microscopic articular cartilage degeneration in guinea pigs with spontaneous osteoarthritis. Osteoarthritis Cartilage 21(4), 574–581 (2013)
35. Wolff, J.: Das gesetz der transformation der knochen. The law of bone remodelling (1892)
36. Woloszynski, T., Podsiadlo, P., Stachowiak, G., Kurzynski, M.: A signature dissimilarity measure for trabecular bone texture in knee radiographs. Med Phys 37(5), 2030–2042 (2010)
37. Zhang, Z., Li, Z., Jiang, L., Jiang, S., Dai, L.: Micro-ct and mechanical evaluation of subchondral trabecular bone structure between postmenopausal women with osteoarthritis and osteoporosis. Osteoporos Int 21(8), 1383–1390 (2010)